Residual welding stress of I-section members beyond the limits of width-thickness ratio

Zhiyuan Li
Chongqing Water Resources and Electric Engineering College, Yongchuan, Chongqing, 402160, China
1628607391@qq.com

Zhiyun Zhao
Shaanxi Architectural Design & Research Institute Co., Ltd, Xi'an, Shaanxi, 710018, China
33005652@qq.com

ABSTRACT. Despite the extensive studies on the effect of width-thickness ratio and residual stress on member behavior, few scholars have probed into the residual stress distribution on the I-section members. Based on the principle of blind hole drilling, this paper conducts an experimental study of the residual welding stresses of eight welded I-shaped members. Through the analysis of the test results, the author draws the following conclusion: it is safe to use I-section members beyond the limits of width-thickness ratio because the residual stress distribution is not severely affected by width-thickness ratio.

KEYWORDS. Steel structure; Residual stress; Material grade; Width-thickness ratio; principle of blind hole drilling; I-shaped members.

Citation: Li, Z., Zhao, Z., Residual welding stress of I-section members beyond the limits of width-thickness ratio, Frattura ed Integrità Strutturale, 41 (2017) 378-387.

Received: 14.03.2017
Accepted: 14.05.2017
Published: 01.07.2017

INTRODUCTION

In many large steel structures, the flexural members are often I-shaped members with excessively high width-thickness ratio. Such members fall into the category of large welded components. After welding, residual welding stress will generate inside the components, producing welding deformation or cracks. When members are subjected to external loads, the local regional stress will grow exponentially under the combined effect of welding stress and external stress, leading to plastic deformation, cracking, and even overall fracturing [1-3].

The residual stress distribution and the size of I-shaped members vary significantly as a result of the effect of the residual stress on structural rigidity, stability, strength and stress corrosion cracking. It is therefore necessary to study the relationship between residual stress distribution and width-thickness ratio of such members. Many Chinese scholars have probed into the effect of width-thickness ratio and residual stress on member behavior. Through the analysis of I-section members, Shang Fan et al. [4] discovered that the residual stress around the weak axis is greatly influenced by the bearing capacity of the component. Huan Xinyuan et al. [5] adopted segmentation method to cut an I-section member into strips, measured the release of residual strain, and constructed a simplified model that can accurately describe the size of stainless steel I-section member and the distribution of residual stress. Qu Lihua [6] simulated the vibration mode and frequency variation

under the influence of residual stress, pointing out that the effect of residual stress on structural mode is too big to be ignored. Taking the Chunyi Bridge on Haihe River as an example, Ding Daiwei et al. [7] expounded the test principle of blind hole method, examined the impact of welding residual stress on the steel box girder bridge, and obtained the distribution and features of the welding residual stress. Mo Mingchao [8] contoured the internal residual stress in welds by cutting open the vertical welding seam, and conducted contour precision testing and fitting.
In the principle of blind hole drilling, this paper aims to measure residual stress, draw residual stress distribution maps, and analyze the influencing factors of welding residual stress, thereby providing a basis for the design of similar components.

TEST OVERVIEW

Test materials

There are 8 specimens in this research, numbered from CH-1 to CH-8. Specimens CH-1~CH-5 are made of the material Q235B, while specimens CH-6~CH-8 are made of the material Q345B. See Tabs. 1 and 2 below for the chemical compositions and mechanical properties of the two types of materials.

Material	Chemical composition (%)					
	C	Si	Mn	P	S	Alt
Q345B	0.069	0.472	0.86	0.014	0.002	0.021
Q235B	0.18	0.029	0.42	0.018	0.003	0.025

Table 1: The chemical compositions of test materials

Material	Mechanical properties			
	σ_y/MPa	σ_s/MPa	δ/%	Impact properties/J
Q345B	460	530	29.5	104
Q235B	335	450	33	115

Table 2: The mechanical properties of test materials

Test equipment

The HK21B type residual stress detector (Fig. 1) and 3-element rosette strain gauge BX120-3CA are adopted for the test.

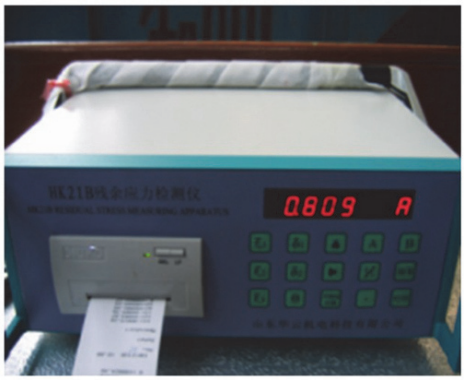

Figure 1: HK21B residual stress detector

Specimen design

Eight welded I-shaped members (CH-1 ~ CH-8) are prepared for the test. The thickness of the specimens varies: CH-1 ~ CH-3 and CH-6 ~ CH-8 are 6mm thick; CH-4 and CH-5 are 10mm thick. Fig. 2 illustrates the specimen sizes and Fig. 3 displays the sizes and width-thickness ratios of the specimens.

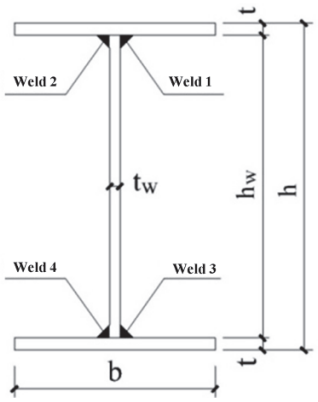

Figure 2: Specimens sizes

Specimen	b/t	h_w/t_w	b/mm	h_w/mm	h/mm
CH-1	14.5	75	180	450	462
CH-2	14.5	125	180	750	762
CH-3	24.5	100	300	600	612
CH-4	24.5	75	300	750	770
CH-5	41.2	100	500	1000	1020
CH-6	14.5	75	180	450	462
CH-7	14.5	125	180	750	762
CH-8	24.5	100	300	600	612

Table 3: Specimen sizes and width-thickness ratios.

Fundamentals

The principle of blind hole residual stress measurement is shown in Fig. 3. If a structural member is subjected to a residual stress field and an elastic strain field, the residual stress at any point inside the small blind hole will be released. As the original stress field falls out of balance, there will be a certain amount of strain release around the blind hole so that the original stress field reaches a new equilibrium. The formation of new stress and strain fields at the residual stress measuring points can be measured by the following formulas [9-11].

$$\sigma_{1,2}=\frac{\varepsilon_1+\varepsilon_3}{4A}\pm\frac{1}{4B}\sqrt{\left(\varepsilon_1-\varepsilon_3\right)^2+\left(2\varepsilon_2-\varepsilon_1-\varepsilon_3\right)^2} \tag{1}$$

$$\sigma_Z=\frac{\sigma_1+\sigma_2}{2}+\frac{\left|\sigma_1-\sigma_2\right|}{2}\cos\left(2\varphi\right) \tag{2}$$

$$tg\left(2\varphi\right)=\frac{\left(\varepsilon_1+\varepsilon_3\right)-2\varepsilon_2}{\varepsilon_1-\varepsilon_3} \tag{3}$$

$$A=-\frac{1+\mu}{2E}\frac{a^2}{r_1r_2}$$

$$B=-\frac{1}{E}\frac{2a^2}{r_1r_2}\left[1+\frac{1+\mu}{4}\frac{a^2\left(r_1^2+r_1r_2+r_2^2\right)}{r_1^2r_2^2}\right] \tag{4}$$

The symbols are explained as below [12]:

ε_1, ε_2 and ε_3: the relieved strain measured by each of the rosettes in the strain ($\mu\varepsilon$);

A, B: the strain release coefficients obtained based on tensile experimental calibration or theoretical calculation formulas based on aperture, hole depth, geometry size of strain rosette and elastic modulus;

θ: the clockwise angle between the maximum principal stress and the stress reference axis of 1# rosette;

σ_1, σ_2: the principle stresses (MPa).

E: the elasticity modulus; μ: the Poisson's ratio;

d, r_1, r_2: the aperture of the blind hole, the distance from the blind hole center to the near end of the strain gauge, and the distance from the blind hole center to the far end of the strain gauge (mm).

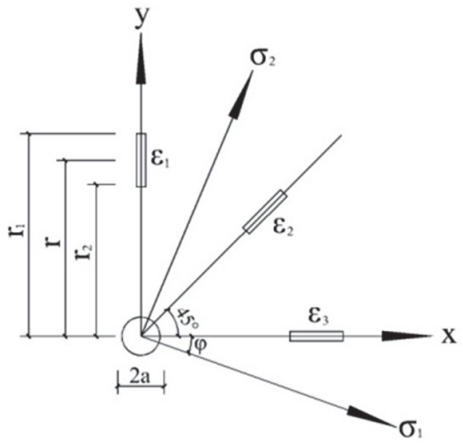

Figure 3: Principle of blind hole drilling method

Residual stress test

Test Methods

Targeted at measuring the distribution of longitudinal residual stress in the I-section members, the rosettes are arranged along the centerline of the cross-section of each specimen [13-21]. For the sake of simplicity, only the rosettes at the upper flange and web are taken into consideration because the cross-section is symmetrical. The rosette arrangement is shown in Figure 3. The spacing between the rosette and the flange is 1/4b; the spacing between the rosette and the web is: 1/6hw (CH-3, CH-4), 1/8hw (CH-5), and 1/4hw (others). The distance from the flange to the edge of the member is 10m, and the distance from the web to the edge of the member is 20mm.

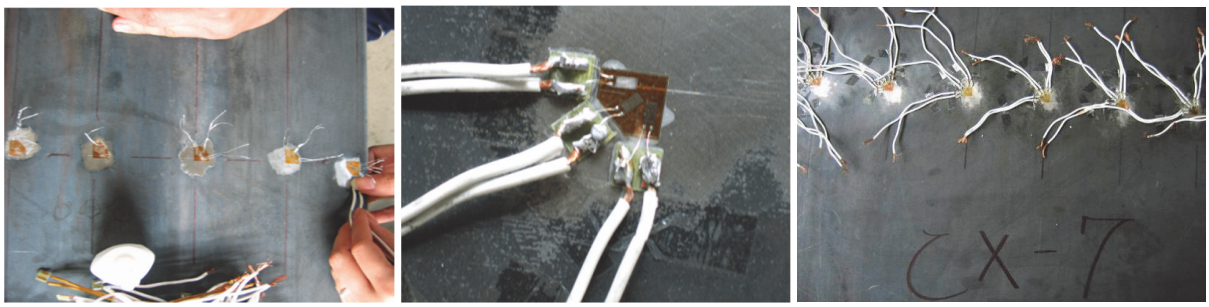

(a) Paste strain rosettes (b) Weld the wires (c) Drill the holes

Figure 4: Strain rosettes cementing, wire welding and drilling

Test Procedure

Following the blind hole drilling method, the test procedure goes as: prepare the surface, paste strain rosettes, weld the wires, install the tool, drill the holes, record the drilling, remove the tool and sort out the tool.
Fig. 4 presents the most important steps in the procedure.

TEST RESULTS AND ANALYSIS

Test results

Figs. 5-12 show the distribution of the longitudinal stresses in the specimens.

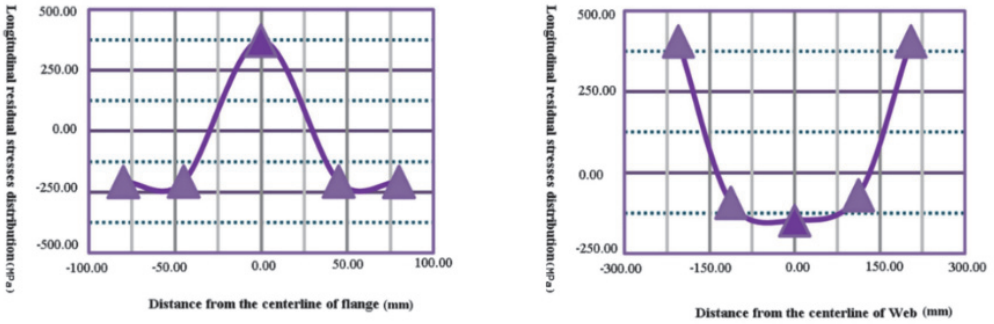

(a) (b)

Figure 5: Longitudinal residual stress distribution of CH-1. (a) Flage; (b) Web.

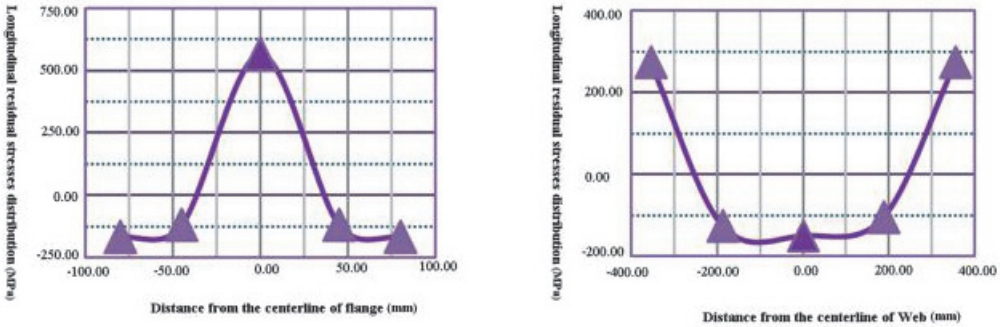

(a) (b)

Figure 6: Longitudinal residual stress distribution of CH-2. (a) Flage; (b) Web.

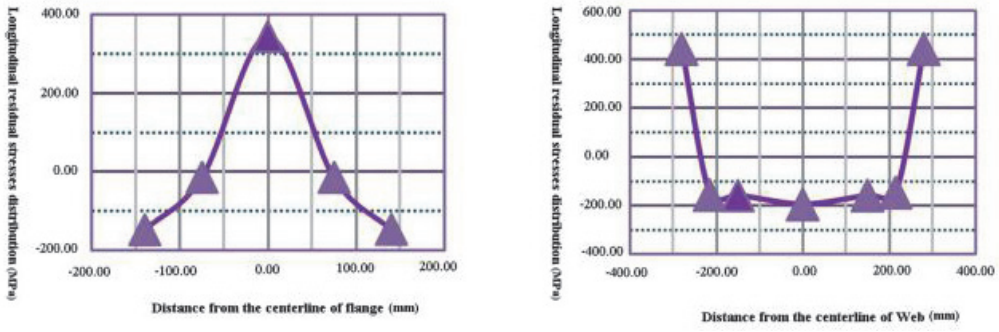

(a) (b)

Figure 7: Longitudinal residual stress distribution of CH-3. (a) Flage; (b) Web.

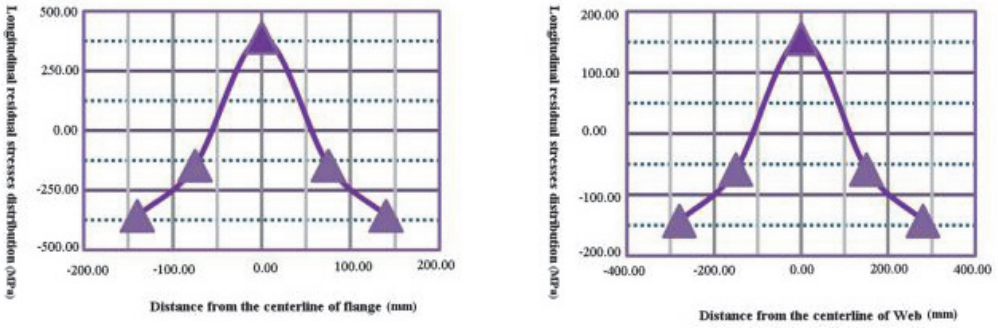

(a) (b)

Figure 8: Longitudinal residual stress distribution of CH-4. (a) Flage; (b) Web.

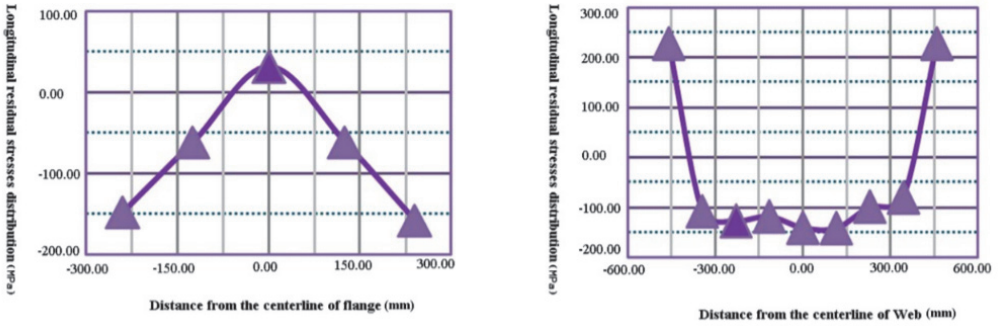

(a) (b)

Figure 9: Longitudinal residual stress distribution of CH-5. (a) Flage; (b) Web.

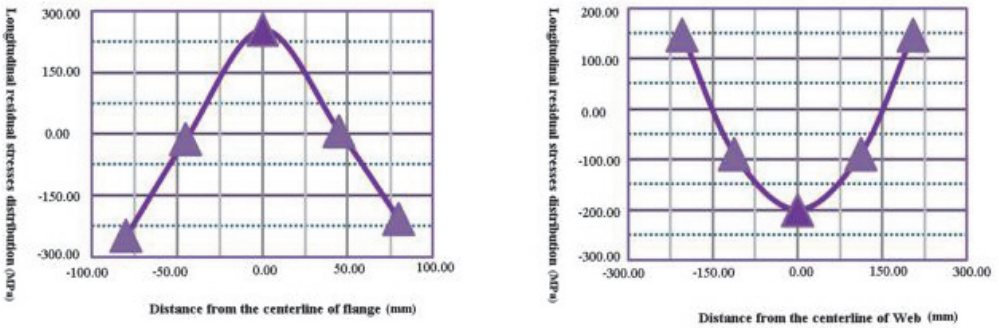

(a) (b)

Figure 10: Longitudinal residual stress distribution of CH-6. (a) Flage; (b) Web.

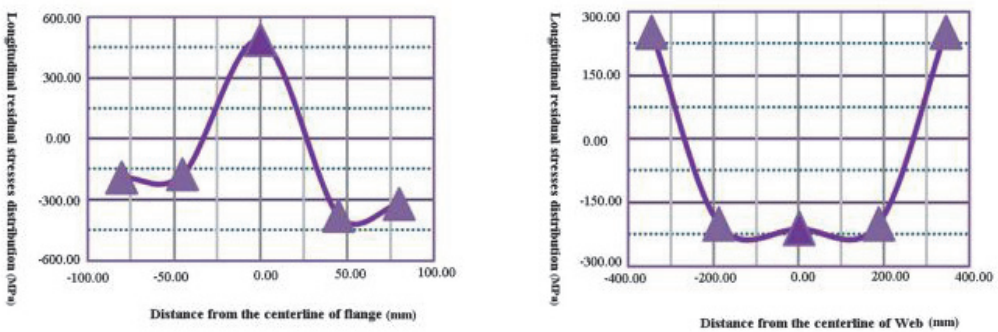

(a) (b)

Figure 11: Longitudinal residual stress distribution of CH-7. (a) Flage; (b) Web.

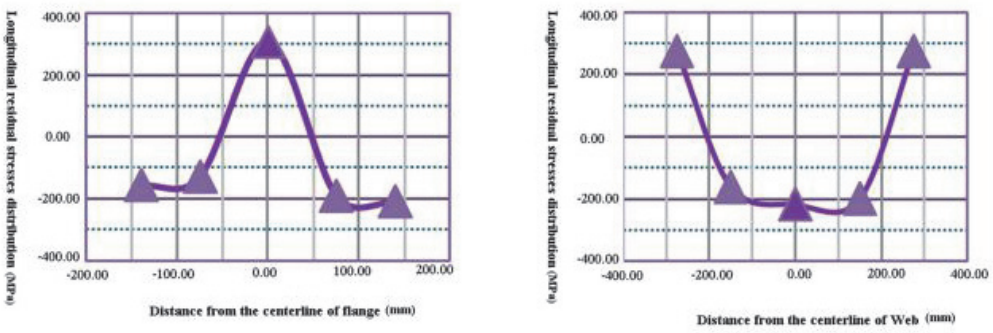

(a) (b)

Figure 12: Longitudinal residual stress distribution of CH-8. (a) Flage; (b) Web.

Analysis of test results

As shown in Figs. 5~12, the residual stress along the centerline in the cross-section obeys symmetric parabolic distribution. In all the specimens, the residual tensile stress descends from the near-weld region to the middle of the member, but the trend is not linear.

The residual tensile stress peaks at the centerline of the member. Except for specimen CH-5, each of the specimens boasts a peak value of residual tensile stress so large as to exceed the yield strength of the material. The peaks of residual tensile stress at the web occur near the edge of weld instead of the flange. With only a few specimens surpassing the yield strength of the material, the web has a small residual tensile stress that essentially follows symmetric parabolic distribution similar to that of the cross-section of I-section members beyond the limits of width-thickness ratio. The stress distribution is basically linear in the middle of the web.

Figs. 13, 14 and 15 make pair-wise comparison of residual stress distributions between CH-1 and CH-6, CH-2 and CH-7, as well as CH-3 and CH-8. Each pair includes two specimens of the same cross-sectional size but different materials. CH-1, CH-2 and CH-3 are made of Q345B, while CH-6, CH-7 and CH-8 are made of Q235B.

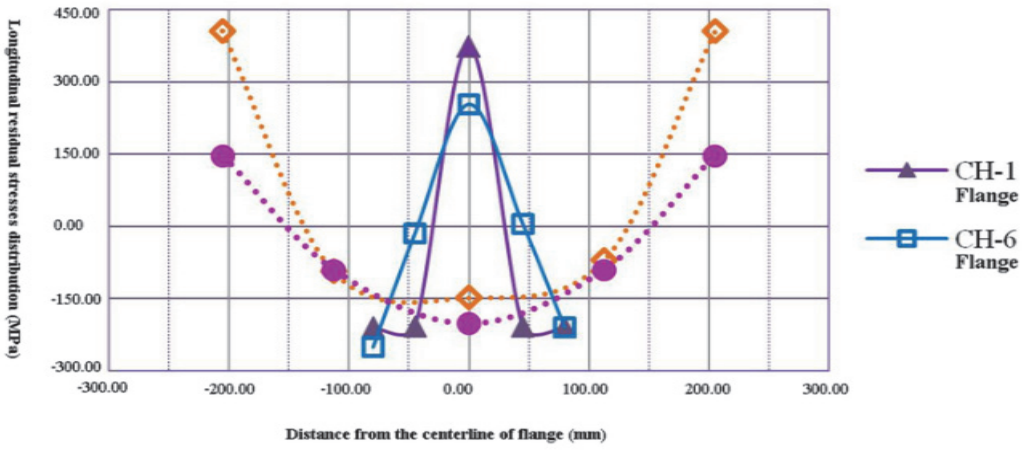

Figure 13: Comparison of residual stress distribution between CH-1 and CH-6.

Influence of yield strength

The material parameters stand for the important influencing factors of welding residual stress. This research mainly emphasizes on the yield strength of Q235B and Q345B in each pair of specimens. As mentioned above, out of the eight specimens CH-1~CH-8, CH-1~CH-5 are made of Q345B, and CH-6~CH-8 are made of Q235B.

Fig. 13 compares the residual stress distributions between CH-1 and CH-6. The two specimens share same cross-sectional size.: 180×450×6×6mm. The materials of CH-1 and CH-6 are Q345B and Q235B, respectively.

According to Fig. 13, the residual stress distribution of the two specimens are largely the same. The only difference lies in the peak residual stress, which is mainly attributable to the difference in materials. Moreover, the peak residual tensile stress at the flange increases from 253.38 MPa in CH-6 to 373.15 MPa in CH-1, up by 47%; the peak residual tensile stress at the

web rises from 147.10 MPa in CH-6 to 405.53 MPa in CH-1, up by 175%. Fig. 14 (comparing CH-2 with CH-7) and Fig. 15 (comparing CH-3 with CH-8) show the same trend. Therefore, the peak residual stress will increase with the yield strength of the material if the cross-section remains the same.
In short, the effect of material grade on residual stress is: for a given width-thickness ratio, the higher the yield strength, the larger the peak value of the residual stress.

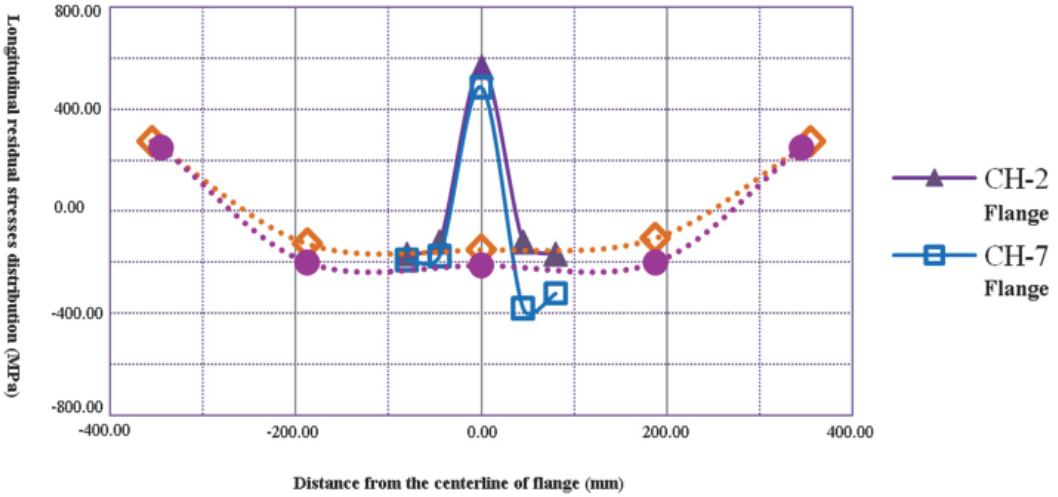

Figure 14: Comparison of residual stress distribution between CH-2 and CH-7.

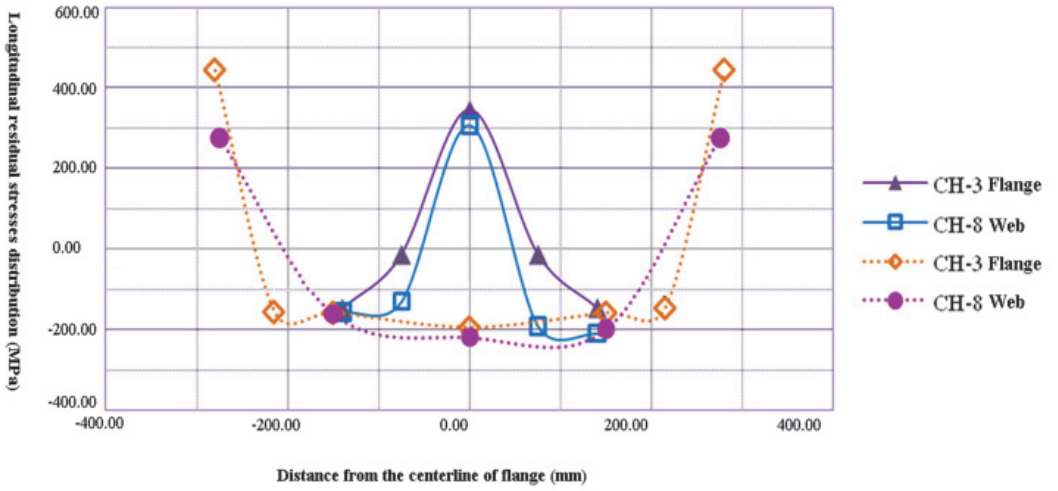

Figure 15: Comparison of residual stress distributions between CH-3 and CH-8.

Influence of material size

Fig. 16 compares the peak residual stresses of three groups of specimens. In each group, the specimens share the same material grade but differ in width-thickness ratio. Specifically, the first and second groups have different width-thickness ratios at the web; the third group have different width-thickness ratios at the flange.
The first group of specimens are CH-1 and CH-2, both of which are made of the same material Q345; however, the two specimens differ in width-thickness ratio at the web (75 vs. 125). The second group of specimens are CH-7 and CH-8, both of which are made of the same material Q235; however, the two specimens differ in width-thickness ratio at the flange (125 vs. 100).
The difference between the two groups of specimens is clearly illustrated in the above figure. For specimens of the same material grade, the peak value of residual stress at the web decreases significantly as the width-thickness ratio increases. For instance, the peak residual stress at the web drops from 405.53MPa in CH-1 to 274.52MPa in CH-2, down by 32%; the peak residual stress at the web falls from 275.23MPa in CH-8 to 251.48MPa in CH-7, down by 9%.

The first group of specimens are CH-2, CH-4 and CH-5, all of which are made of the same material Q345; however, the three specimens differ in width-thickness ratio at the flange, respectively 14.5, 24.5 and 41.2.

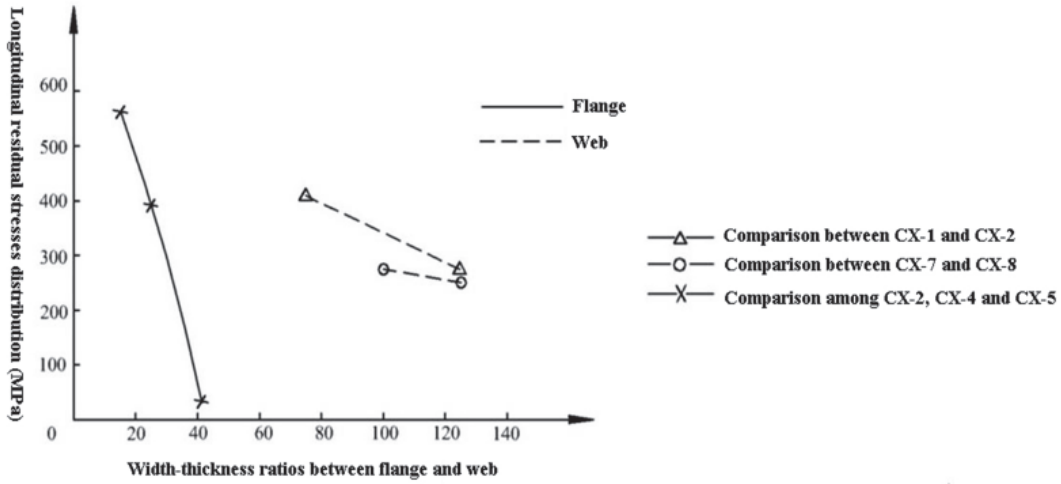

Figure 16: The relationship between the peak residual tensile stress and width-thickness ratio

The difference between the third of specimens is also presented in the above figure. For specimens of the same material grade, the peak value of residual stress at the flange plunges with the increase of the width-thickness ratio. In particular, the peak residual stress falls all the way from 564.06MPa in CH-2, 388.09MPa in CH-4 to 31.16MPa in CH-5.
The increase in width-thickness ratio means the member is getting thinner and the sectional size (width) is getting larger. The test results reveal the weakening of the effect of residual welding stress on member behavior and the shrinkage of peak residual stress in the cross-section. In other words, the width-thickness ratio has an insignificant effect on the distribution of residual stress in welded I-section members. Therefore, it is safe to use large I-section members beyond the limits on width-thickness ratio.

Conclusion

Following the blind-hole drilling method, this paper explores the effect of width-thickness ratio on the behavior of I-section members. The conclusion are as follows:
(1) It is safe to use large I-section members beyond the limits on width-thickness ratio.
(2) For a given width-thickness ratio, the higher the yield strength, the larger the peak value of the residual stress.
(3) For structural members of the same grade, the larger the width-thickness ratio, the smaller the peak residual stress.

Acknowledgements

The research of this paper is made possible by the generous support from the Special Fund for Construction of Key Disciplines in Shaanxi Province, China (No.: E01001, E01003), key research project of Chongqing Water Resources and Electric Engineering College (No.: K201615), and the Science and Technology Project Affiliated to the Education Department of Chongqing Municipality (No.: KJ1603604).

References

[1] The Ministry of Construction of the People's Republic of China, GB 50017-2003 Code for Design of Steel Structures, Beijing: China Planning Press——Steel structure design specification, GB 50017-2003, 2013.
[2] Teng, T.L., Fung, C.P., Chang P.H., Yang W.C., Analysis of residual stresses and distortions in T-joint fillet welds, Int. J. Pres. Ves. Pip., 78 (2001) 523-538. DOI: 10.1016/S0308-0161(01)00074-6.

[3] Park, M.J., Yang, H.N., Jang, D.Y., Kim, J.S., Jim, T.E., Residual stress measurement on welded specimen by neutron diffraction, Mater Process Tech., 155-156 (2004) 1171-1177. DOI: 10.1016/j.jmatprotec.2004.04.393.
[4] Shang, F., Zhao M.H., Stainless steel overall stability of i-section section axial compression member finite element study, Journal of engineering mechanics, 33(3) (2016) 112-119.
Yuan, H.X., Wang, Y.Q., Shi, Y.J., The stainless steel welded i-section experimental study the residual stress distribution, Journal of building structures, 35(6) (2014) 84-92.
[5] Qu, L.H., Wei, F.F., Huang, J.H., At the beginning of bending and residual stress of welding steel i-beam modal effect of numerical simulation, Journal of water conservancy and architectural engineering, 11(1) (2013) 105-109.
[6] Ding D.W., Xue J., Blind hole method in the application of steel box girder bridge welding residual stress test, Journal of urban road and bridge and flood control, 2 (2017) 158-161.
[7] Mo, M.C., The internal residual stress in weldments was tested based on contour method, Journal of low-carbon technologies, 2 (2017) 67-68.
[8] American Society for Testing and Materials, Standard Test Method for Determining Residual Stresses by the Hole-drilling Strain-gage Method, America: Annual Book of ASTM Standards, E837-E808, 2008.
[9] Trebuna, F., Simcak, F., Bocko, J., Sarga, P., Trebuna, P., Pastor M., Mihok, Quantification of Residual Stresses in the Weld by the Hole-drilling Method, Metalurgija, 47(2) (2008) 133-137.
[10] Kamal, B.S., Farahaninia, Experimental measurement of residual stresses in cold-drawn aluminum tubes, USA: The Graduate Faculty of Texas Tech University 13 (1990).
[11] Wang, N., Research on measuring welding residual stress of plate of moderate thickness using blind hole method, Dalian University of Technology, Dalian, (2007).
[12] Chen, X.R., Jiang Y.Y., Zhao Z.Y., Comparison for Different Circumferential Weld-induced Imperfections on Steel Silos. Advanced Materials Research, (2011) 250-253. DOI: 10.4271/910191.
[13] Tsai, C.L., Dai, W.L., Dickinson, D.W., Analysis and Development of a Real-time Control Methodology in Resistance Spot Welding, Welding Research Supplement, 70(12) (1991) 339-351. DOI: 10.4271/910191.
[14] Inoue, T., Metallo-Thermo-Mechanics Application to Phase Transformation Incorporated Processes, Pros. Theoretical Prediction in Joining and Welding, 12(3) (1996) 89-112.
[15] Lars-Erik, L., Lennart K., Deformations and Stresses in Welding of Shell Structures, International Journal for Numerical Methods in Engineering, 25(2) (1998) 635-638. DOI: 10.1002/nme.1620250223.
[16] Teng, T.L., Analysis of Residual Stresses and Distortions in T-joint Fillet Welds, International Journal of Pressure Vessels and Piping, 78(8) (2001) 523-538. DOI: 10.1016/S0308-0161(01)00074-6.
[17] Sicot, O., Gong, X.L., Cherouat, A., Lu, J., Influence of Experimental Parameters on Determination of Residual Stress Using the Incremental Hole-drilling Method, Composites Science and Technology, 64(2) (2004) 171-180. DOI: 10.1016/S0266-3538(03)00278-1.
[18] American Society for Testing and Materials. ASTM E837—08: Standard Test Method for Determining Residual Stresses by the Hole-drilling Strain-gage Method, America: Annual Book of ASTM Standards, (2008).
[19] Cui, X.W., Ni, W., Ren, C., Early Hydration Kinetics of Cementitious Materials Containing Different Steel Slag Powder Contents, International Journal of Heat and Technology, 34(4) (2016) 590-596. DOI: 10.18280/ijht.340406.
[20] Wang, X.Z., Wang, C.Q., Analysis of Temperature Stress in Control of Bridge Construction, International Journal of Heat and Technology, 34(4) (2016) 715-721. DOI: 10.18280/ijht.340423.